Catalysis Science & Technology

Accepted Manuscript

ROYAL SOCIETY OF CHEMISTRY

www.rsc.org/catalysis

Cite this: DOI: 10.1039/c0xx00000x

www.rsc.org/xxxxxx

ARTICLE TYPE

Hydrothermal Synthesis of Zinc Indium Sulfide Microspheres with Ag^+ doping for Enhanced H_2 Production by Photocatalytic Water Splitting under Visible Light

Fan Li, [a] Jianheng Luo, [a] Guoping Chen, [a] Yuzun Fan, [b] Qingli Huang, [a] Yanhong Luo, [a] Dongmei Li *[a] and Qingbo Meng *[a]

Received (in XXX, XXX) Xth XXXXXXXXX 20XX, Accepted Xth XXXXXXXXX 20XX
DOI: 10.1039/b000000x

Two series of $ZnIn_xS_{1+1.5x}$ solid solution and Ag(y)-$ZnIn_xS_{1+1.5x+0.5y}$ are prepared by hydrothermal method. The synthetic conditions such as the molar ratio of In/Zn, the pH value, hydrothermal temperature and reaction time are found to intensely influence the crystal structure, the morphology of the photocatalyst as well as its phototcatalytic activity for H_2 generation from water. It is revealed that the $ZnIn_{1.5}S_{3.25}$ solid solution (In/Zn = 1.5) prepared at 160 ^oC for 6 h by adding 1 mL hydrochloric acid in the precursor solution shows a highest photocatalytic H_2 evolution rate of 1.85 mmol $ħ^{-1}$ g^{-1} in the presence of Ru co-catalyst and Na_2S/Na_2SO_3 as sacrificial reagents. Furthermore, after Ag^+ doping, the photocatalytic H_2 evolution rate has been remarkably increased to 3.20 mmol $ħ^{-1}$ g^{-1} for Ag(1.5%)-$ZnIn_{1.5}S_{3.2575}$ sample. This work provides a new opportunity to develop efficient photocatalysts for photosplitting water into hydrogen.

Introduction

Since Honda-Fujishima effect of water splitting on TiO_2 electrode was discovered in 1972, photocatalytic hydrogen production from water has attracted world-wide interests.[1, 2] To realize highly efficient water photosplitting into hydrogen, much effort has been focusing on developing various photocatalysts, especially with visible-light response, because the visible light constitutes 43% of the solar energy.[3-5] In recent years, inorganic semiconductor CdS has been developed as promising visible-light driven photocatalysts due to its narrow band gaps and high absorption coefficients.[6-8] However, pure CdS exhibits extremely low photocatalytic activity and suffers photocorrosion during the photo-reactions as well.[9] Tremendous efforts have been devoted to solve the above problems, such as co-catalyst loading[8, 10-13], forming junctions between CdS and another semiconductor[14, 15], loading CdS nano-particles on mesoporous materials[16, 17], *etc*. Recently, Li and co-workers reported PdS-Pt/CdS with the highest apparent quantum efficiency of 93% for photocatalytic water splitting of hydrogen production.[8] However, the practical application of CdS photocatalysts will be limited by the environmental contamination.[9] Therefore, it is necessary to design and synthesize more stable and enviromentally friendly photocatalysts.

Ternary Zn-In-S solid solutions with the stoichiometric ratio (Zn:In:S= 1: 2: 4) have been widely investigated as potential eco-friendly visible-light-driven photocatalysts with relatively low toxicity.[18-23] Li and co-workers firstly reported $ZnIn_2S_4$ can exhibit a steady photocatalytic activity for phtocatalytic water splitting to produce H_2 over 150 hours.[18] Li and Bai synthesized hexagonal $ZnIn_2S_4$ porous microspheres with high specific surface area of 165.4 m^2 g^{-1} through a CPBr-assisted hydrothemal method, which showed 766.8 μmol·h^{-1} g^{-1} of H_2 evolution rate.[24] Li and Chen synthesized cubic $ZnIn_2S_4$ nanoparticles and hexagonal $ZnIn_2S_4$ flower-like microspheres *via* a facile hydrothermal method by changing the metal precursors and found that the cubic phase can perform better photocatalytic activity than hexagonal phase.[25] Qian and co-workers found that the increase of {006} facets of hexagonal $ZnIn_2S_4$, terminated by metal ions, can improve their photocatalytic H_2 evolution rate to 220.45 μmol·h^{-1}.[26] Guo's group synthesized Cu^{2+} and Ni^{2+} doped $ZnIn_2S_4$ microspheres *via* hydrothermal processes, which photocatalytic activity were much higher than that of the un-doped $ZnIn_2S_4$.[27, 28] However, few works have been reported about the influence of different In/Zn ratios and other transition metal ion doping (such as Ag^+) on the photocatalytic property of the Zn-In-S solid solution.

Herein, Zn-In-S solid solution (labeled as $ZnIn_xS_{1+1.5x}$) and Ag^+ doped Zn-In-S solid solution (labeled as Ag(y)-$ZnIn_xS_{1+1.5x+0.5y}$) were prepared by hydrothemal method. The photocatalytic activities of the two series of photocatalysts for water splitting into hydrogen are evaluated under visible-light illumination in the presence of Na_2S/Na_2SO_3 as sacrificial reagents and Ru as the co-catalyst. The synthetic conditions such as the molar ratio of In/Zn, the pH value, hydrothermal temperatures and reaction time were systematically studied to investigate their influence on the morphologies of the photocatalsts and the photocatalytic activities for hydrogen evolution. Besides, after Ag^+ doping, the photocatalytic H_2 evolution rate has been remarkably improved to

3.20 mmol h^{-1} g^{-1} for Ag(1.5%)-$ZnIn_{1.5}S_{3.2575}$ solid solution, in comparison to 1.85 mmol h^{-1} g^{-1} for corresponding $ZnIn_{1.5}S_{3.25}$ solid solution.

Experimental

Reagents and Chemicals

All of the reagents were used without further purification. Silver nitrate ($AgNO_3$, AR, 99.8%), Na_2S $9H_2O$ (AR, 98%) and Na_2SO_3 (AR, 97%) were from Xilonghuagong, indium nitrate ($In(NO_3)_3$ $4.5H_2O$, 99.5%), zinc nitrate ($Zn(NO_3)_2$ $6H_2O$, AR, 99%), thioacetamide (C_2H_5NS, AR, 99%) and $RuCl_3$ xH_2O (At least 37 wt% Ru) from Sinopharm.

Synthesis of $ZnIn_xS_{1+1.5x}$ solid solution and Ag(y)-$ZnIn_xS_{1+1.5x+0.5y}$ samples

In a typical synthesis of $ZnIn_xS_{1+1.5x}$ solid solution samples, 30 mL of metal nitrates aqueous solution with different In/Zn molar ratios (here, $Zn(NO_3)_2$ $6H_2O$ was fixed as 1 mmol) and a double excess of thioacetamide was stirring rigorously to form a homogeneous solution. The pH value of mixed solution was adjusted by using different amount of hydrochloric acid (12mol L^{-1}), which was in the range of 0-3 mL. The mixed solution was then transferred into a 45 mL Teflon-lined autoclave. The autoclave was sealed, maintained at 160 ^oC for 6 hours. After cooling down to room temperature, the reaction mixture was centrifuged to give the precipitate, which was washed with deionized water and ethanol for several times, collected and dried in vacuum oven overnight. For doped solid solution, tiny amount of $AgNO_3$ was added together with In^{3+} and Zn^{2+} into the precursor solution before the hydrothemal reaction. The doping percentage of Ag^+ is defined as the molar ratio of $Ag^+/(In^{3+}+Zn^{2+})$ in the precursor solution, which was in the range of 0-3 %.

Characterization

The X-ray diffraction patterns (XRD) of the samples were obtained by Bruker D8 Advance X-ray diffractometer with Cu-Kα irradiation (λ= 0.154178 nm) at 40 kV and 40 mA. The scan rate is 0.1 ^{o}/s. The surface morphologies of the samples were investigated by a scanning electron microscope (SEM, XL30 S-FEG, FEI). The UV-visible diffuse reflectance spectra (UV-vis DRS) were obtained on UV-visible spectrophotometer (UV-2450, Shimadzu) and were converted from reflection to absorbance by the Kubelka-Munk method. X-ray photoelectron spectroscopy (XPS) was collected on AXIS ULTRA^{DLD} with an Al Kα chromatic X-ray source (1486.6 eV). All binding energies were referred to the C1s peak of 284.8 eV.

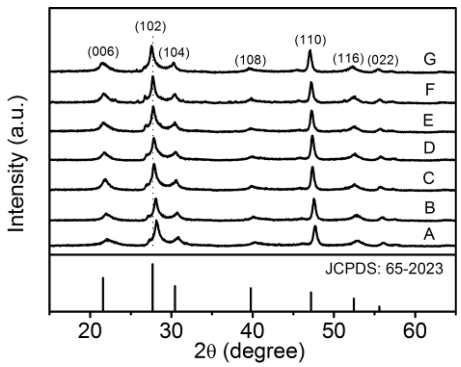

Fig. 1 XRD patterns of $ZnIn_xS_{1+1.5x}$ solid solution samples prepared by adding 1 mL hydrochloric acid at 160 ^oC for 6 h. The x values of samples are (A) 0.8; (B) 1.0; (C) 1.2; (D) 1.5; (E) 1.8; (F) 2.0; (G) 3.0.

Photocatalytic Activity Measurement

The photocatalytic reactions were carried out in a Pyrex reaction cell connected to a home-made closed gas circulation and evacuation system. 0.1 g photocatalyst powder was ultrasonically dispersed for 10 min in a 100 mL aqueous solution containing 0.35 M Na_2S and 0.25 M Na_2SO_3 as sacrificial reagents. Then the suspension was thoroughly degassed and irradiated by a 300 W Xe lamp (PLS-SXE300, Trusttech) equipped with an optical filter (λ ≥ 420 nm) to cut off ultraviolet light and a water filter to remove infrared light. Ru co-catalyst was *in situ* deposited according to the reference, that is, the reaction mixture with 0.5 wt% of $RuCl_3$ xH_2O (metal basis) was irradiated under Xe lamp with full spectrum for 30 min before the H_2 production measurement.[29] The evolved H_2 amount was determined by an on-line gas chromatography with a thermal conductivity detector (Varian, CP3800, molecular sieve 5Å column, Ar carrier). The photocatalytic activities were compared by the average H_2 evolution rate in the first 5 hours.

Results and discussion

XRD patterns of $ZnIn_xS_{1+1.5x}$ solid solution samples with different molar ratios and Ag(y)-$ZnIn_{1.5}S_{3.25+0.5y}$ samples with different doping amount

Fig. 1 shows the X-ray diffraction patterns of the $ZnIn_xS_{1+1.5x}$ samples with different In/Zn compositions, which preparation condition is using 1 mL hydrochloric acid to adjust pH value, then hydrothermally at 160 ℃ for 6 hour. It is found that the single phase of a hexagonal structure (JCPDS: 65-2023) is obtained for all the samples, which is in agreement with the literature.[25, 30] With the value of x increasing, the (102) diffraction peak shows a successive shift to lower angle, indicating that the samples are the $ZnIn_xS_{1+1.5x}$ solid solution, instead of a simple mixture of In_2S_3 and ZnS. Similar diffraction patterns were reported in previous work about ternary or multinary sulfide systems.[31, 32] The influence of different amounts of hydrochloric acid in the preparation process on the composition of $ZnIn_{1.5}S_{3.25}$ is also investigated (Fig. S1). It can be

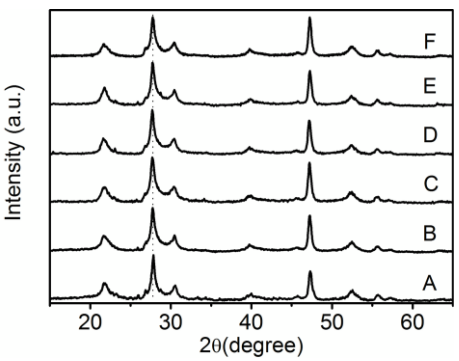

Fig. 2 XRD patterns of Ag(y)-$ZnIn_{1.5}S_{3.25+0.5y}$ solid solution samples prepared by different Ag^+ doping amount at 160 ℃ for 6 h with 1 mL hydrochloric acid added. The Ag^+ doping amounts are (A) 0; (B) 0.5 %; (C) 1.0 %; (D) 1.5 %; (E) 2.0 %; (F) 3.0 %. The plot A is the same as the plot D in Fig. 1.

Cite this: DOI: 10.1039/c0xx00000x

www.rsc.org/xxxxxx

ARTICLE TYPE

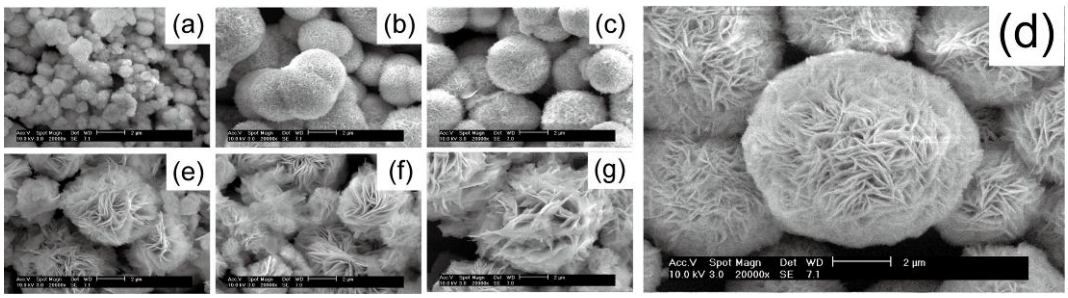

Fig. 3 SEM images of $ZnIn_{1.5}S_{3.25}$ samples prepared by adding different amount of hydrochloric acid at 160 ℃ for 6 h. The amounts of hydrochloric acid are (a) 0 mL; (b) 0.25 mL; (c) 0.5 mL; (d) 1.0 mL; (e) 1.5 mL; (f) 2.0 mL; (g) 2.5 mL. The scale bar is 2 μm.

seen that when no extra hydrochloric acid was added, the diffraction patterns can be indexed to a cubic phase (JCPDS: 48-1778). When 0.25 and 0.5 mL of hydrochloric acid were added, respectively, the hexagonal phase (JCPDS: 65-2023) appears with a relatively low crystallinity, and the solid solutions are indeed the mixture of the two structures. Further increasing hydrochloric acid to 1 mL, the pure hexagonal phase is obtained (plot D in Fig. S1). However, when 1.5 mL or more were added, the unexpected crystal phase of sulfur was observed (marked diffraction peaks in Fig. S1), which is supposed to be disadvantaged to the photocatalytic activities (discussed below). Obviously, the hydrochloric acid significantly influences the crystal structures of $ZnIn_xS_{1+1.5x}$ solid solution, which is in agreement with Li and Chen' work.[25]

Fig. 2 illustrates the XRD patterns of Ag^+ doped samples. No distinct changes for the position of the diffraction peaks are found with the variation of the doping amount. In spite of the ionic size of Ag^+ (1.14 Å) is much larger than that of Zn^{2+} (0.74 Å) and In^{3+} (0.76 Å), however, the doping amount is too little to influence the position of the diffraction peaks significantly.[33]

SEM images of $ZnIn_{1.5}S_{3.25}$ solid solution samples prepared by using different amount of hydrochloric acid and Ag(y)-$ZnIn_{1.5}S_{3.25+0.5y}$ samples with different doping amount

The morphologies of $ZnIn_{1.5}S_{3.25}$ solid solution samples with different amount of hydrochloric acid added are investigated, as shown in Fig. 3. The morphologies are significantly different while adding different amount of hydrochloric acid. Without using hydrochloric acid, the morphology of the $ZnIn_{1.5}S_{3.25}$ samples is micro-particles with irregular shapes (Fig. 3a). It is interesting that $ZnIn_{1.5}S_{3.25}$ samples with 0.25 and 0.5 mL hydrochloric acid show a transitional form in the morphologies. The surface of the microsphere is composed of plate-like hierarchical structures. When adding 1 mL hydrochloric acid before the hydrothermal reaction, the microsphere obtained becomes totally plate-like hierarchical structure with about 5 μm in size. However, this integrated structure is broken when more hydrochloric acid is used. These changes in the morphologies are consistent with the XRD results, indicating that different amounts of hydrochloric acid indeed have a significant influence on the crystal structure and morphology of the solid solution samples. Besides, the morphologies of the $ZnIn_{1.5}S_{3.25}$ samples prepared at different hydrothermal temperature and reaction time at 160 ℃ with 1 mL hydrochloric acid added are investigated by SEM images (shown in Fig. S2). It is found that, the morphologies of the samples prepared with different hydrothermal temperature are similar except the broken of the plate-like hierarchical microsphere for the sample hydrothermally at 200 ℃ (shown in Fig. S2e). A hollow structure is thus suggested from the broken microsphere. Furthermore, the morphologies of the $ZnIn_{1.5}S_{3.25}$ samples prepared for 9 h shows a more disordered structure than the other two samples, as shown in Fig. S3, which may be the

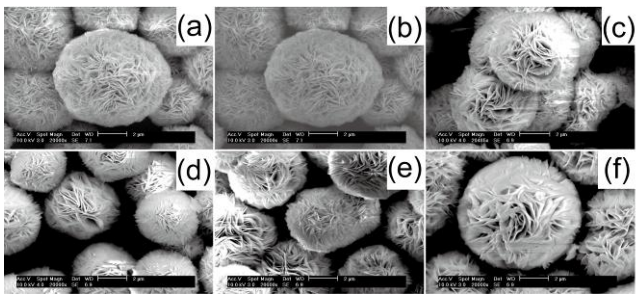

Fig. 4 SEM images of Ag(y)-$ZnIn_{1.5}S_{3.25+0.5y}$ samples prepared with different Ag^+ doping amount at 160 ℃ for 6 h by adding 1 mL hydrochloric acid. The doping amounts are (a) 0; (b) 0.5 %; (c) 1.0 %; (d) 1.5 %; (e) 2.0 %; (f) 3.0 %. The scale bar is 2 μm, and the Fig. 4a is the same figure as the Fig. 3d.

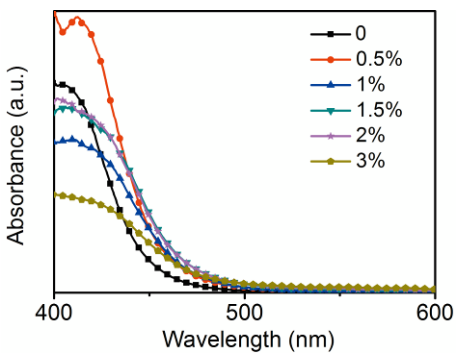

Fig. 5 UV-vis diffuse reflection spectra of Ag(y)-$ZnIn_{1.5}S_{3.25+0.5y}$ samples prepared by adding 1 mL hydrochloric acid at 160 ℃ for 6 h.

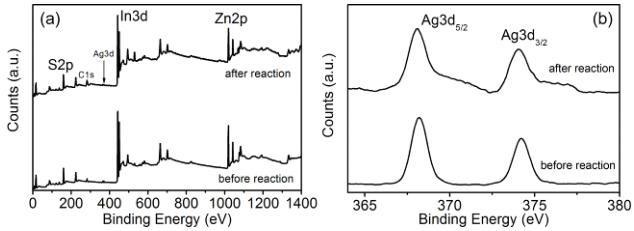

Fig. 6 XPS data collected before and after the photocatalytic H_2 evolution reaction for 15 hours from the surface of the Ag(1.5%)-$ZnIn_{1.5}S_{3.2575}$ sample prepared by adding 1 mL hydrochloric acid at 160 ℃ for 6 h: (a) the survey spectrum; (b) partial spectrum of Ag3d core-level.

reason of the lower photocatalytic H_2 evolution rate in comparison to the samples hydrothermally for 3 h and 6 h. Moreover, Fig. 4 shows the change of morphologies by varying the doping amount of Ag(y)-$ZnIn_{1.5}S_{3.25+0.5y}$ samples. It is found that, the morphologies of the samples prepared with different doping amount are all plate-like hierarchical microsphere without distinct differences.

UV-vis diffuse reflection spectra of Ag(y)-$ZnIn_{1.5}S_{3.25+0.5y}$ samples with different doping amounts

As we know, transition metal ion doping can enhance the charge transfer and photocatalytic activities.[34-38] In this work, a series of Ag^+ doped-$ZnIn_{1.5}S_{3.25}$ samples were prapared, which UV-vis diffuse reflection spectra are given in Fig. 5. Absorption edge of $ZnIn_{1.5}S_{3.25}$ solid solution is about 490 nm, which shows an intense absorption band with a steep edge, indicating that the absorption is assigned to an intrinsic transition from the valence band to conduction band of the solid solution, not the transition from impurity levels.[31] When the $ZnIn_{1.5}S_{3.25}$ solid solution is doped with Ag^+, its visible absorption is red-shifted from 490 to about 600 nm for Ag(3%)-$ZnIn_{1.5}S_{3.265}$. Absorption bands with tails are possibly ascribed to a discontinuous Ag4d level formed in the forbidden band. Besides, the Ag4d donor levels are risen up with the increase of the doping amounts from 0.5% to 3%, resulting in the slight decrease of the band gaps (shown in Table 2). There are no light response belonging to Ag_2S in the region longer than 550 nm for doped solid solution, indicating the exsitence of Ag^+ as a dopant, but not as Ag_2S.

XPS characterization of Ag(1.5%)-$ZnIn_{1.5}S_{3.2575}$ sample

Fig. 6a presents the XPS measurements of Ag(1.5%)-$ZnIn_{1.5}S_{3.2575}$ sample, showing the existence of Ag, In, Zn and S elements in the doped samples. The binding energies for $Ag3d_{5/2}$ and $Ag3d_{3/2}$ before the photocatalytic H_2 evolution reaction are 368.2 and 374.2 eV, respectively (as shown in Fig. 6b), indicating that the oxidation state of silver in the samples is Ag^+, which are in good agreement with that in the literature.[39] Therefore, the formula of Ag doped $ZnIn_xS_{1+1.5x}$ is given as Ag(y)-$ZnIn_{1.5}S_{3.25+0.5y}$ for charge neutrality here. Besides, the binding energies of In3d and Zn2p illustrate that their valence states are In^{3+} and Zn^{2+}, respectively (Fig. S5). In addition, the comparison of the samples before and after the photocatalytic reaction revealed that the binding energies of all the elements do not change, indicating that the doped solid solutions are quite stable in the presence of the sacrificial reagents and under visible light irradiation, and no obviously Ag^0/Ag^+ conversion happens. Moreover, to further ensure the doping position of Ag^+, the X-ray

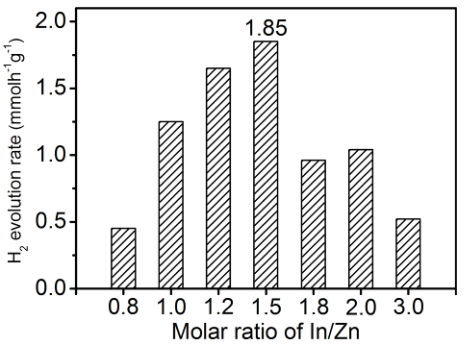

Fig. 7 H_2 evolution rates of as-prepared $ZnIn_xS_{1+1.5x}$ solid solution samples prepared by adding 1 mL hydrochloric acid at 160 ℃ for 6 h.

energy dispersive spectroscopy (XEDS) maps of silver, indium and zinc for Ag(1.5%)-$ZnIn_{1.5}S_{3.2575}$ sample were also investigated, as shown in Fig. S4. The maps reveal that the distribution of all the cations are homogeneous, which further confirms the formation of the doped solid solution.

Photocatalytic activities

The effect of In/Zn molar ratios on the photocatalytic activities of $ZnIn_xS_{1+1.5x}$ solid solutions (Synthetic condition: hydrothermal reaction at 160 ℃ for 6 h, adding 1 mL hydrochloric acid) is evaluated in the presence of Ru (0.5 wt%) co-catalyst and Na_2S/Na_2SO_3 as sacrificial reagents under visible-light irradiation, as shown in Fig. 7. Pure ZnS has almost no hydrogen production. In^{3+} incorporation will lead the activities of the $ZnIn_{0.8}S_{2.2}$ solid solution (x= 0.8) increasing to 0.45 mmol h^{-1} g^{-1}. The highest activity can reach to 1.85 mmol h^{-1} g^{-1} for the sample $ZnIn_{1.5}S_{3.25}$ (x= 1.5). The increase of the photocatalytic activity is ascribed to an optimal band structure of $ZnIn_xS_{1+1.5x}$ solid solutions with a visible-light response and a negative conduction band level. However, the H_2 evolution rates decrease by further increasing the In^{3+} content. Although the light absorption range is expanded by reducing the band gap, the conduction band position is also lowered, which is unfavorable for water reduction. For comparison, the mixture of In_2S_3 and ZnS with the same atom ratio as $ZnIn_{1.5}S_{3.25}$ sample exhibits only 0.22 mmol h^{-1} g^{-1} of H_2 evolution rate under the same photocatalytic measurement, much lower than that of $ZnIn_xS_{1+1.5x}$ solid solution. This further confirms the formation of solid solution.

Table 1 presents the influence of different amounts of hydrochloric acid added, hydrothermal temperature and hydrothermal reaction time for the preparation process on the photocatalytic activities of $ZnIn_{1.5}S_{3.25}$ samples. It is meaningful that the amount of hydrochloric acid added will influence not only the crystal structure, the morphology of the solid solution, but also the photocatalytic activities. Without using hydrochloric acid before hydrothermal reaction, the resultant sample had only a H_2 evolution rate of 0.36 mmol h^{-1} g^{-1}. After adding hydrochloric acid, the H_2 evolution rate increases intensely to as high as 1.85 mmol h^{-1} g^{-1}. Besides, when hydrothermal reactions were carried out in the range of 120-180 ℃, the photocatalytic activities of resultant samples are quite similar. However, further increasing the temperature to 200 ℃, the photocatalytic activity will decrease significantly. These phenomena are not the same as that reported by Chai and Peng who found that the pH value and hydrothermal temperature had no such distinguished effects on

Table 1 Summary of the amount of added hydrochloric acid, hydrothermal temperature, hydrothermal reaction time and photocatalytic activities of $ZnIn_{1.5}S_{3.25}$ solid solution photocatalysts.

HCl/mL	Hydrothermal temperature/°C	Reaction time/h	H_2 evolution rate [a]/mmolh^{-1}g^{-1}
0	160	6	0.36
0.25	160	6	0.71
0.5	160	6	0.94
1.0	160	6	1.85
1.5	160	6	0.96
2	160	6	0.92
2.5	160	6	0.79
1.0	200	6	0.75
1.0	180	6	1.70
1.0	140	6	1.83
1.0	120	6	1.76
1.0	160	3	0.60
1.0	160	9	1.44

[a] Catalysts, 0.1 g; reactant solution, 100 mL aqueous solution containing 0.35 M Na_2S and 0.25 M Na_2SO_3 as sacrificial reagents with 0.5 wt% Ru loaded as co-catalyst; light source, 300 W Xenon lamp with a cut-off filter ($\lambda \geq 420$ nm); the H_2 evolution rates are calculated by the average rate of the first five hours.

the photocatalytic activities for H_2 generation.[30]

The photocatalytic activities for H_2 evolution rates of Ag(y)-$ZnIn_{1.5}S_{3.25+0.5y}$ samples are shown in Table 2. All the doped samples can exhibit higher activities than that of the undoped sample, indicating the positive effect of Ag^+ doping on photocatalysts. In the meantime, the H_2 evolution rates are sensitive to the Ag^+ doping amount. When 0.5% Ag^+ is introduced, the H_2 evolution rate dramatically increases to 2.81 mmol $\hbar^{-1}$ g^{-1}. Further increasing doping amounts, the H_2 evolution rate can reach a maximum value of 3.20 mmol $\hbar^{-1}$ g^{-1} for Ag(1.5%)-$ZnIn_{1.5}S_{3.2575}$ sample. In fact, quaternary Ag-In-Zn-S has been studied previously. In our work, 3.20 mmol $\hbar^{-1}$ g^{-1} of hydrogen evolution rate is obtained for Ag(1.5%)-$ZnIn_{1.5}S_{3.2575}$ whereas 0.80 mmol $\hbar^{-1}$ g^{-1} for $(AgIn)_{0.22}Zn_{1.56}S_2$ in Kudo's

Table 2 Influence of the compositions, band gaps on photocatalytic activities of the Ag(y)-$ZnIn_{1.5}S_{3.25+0.5y}$ samples.

Sample/y[a]	Band gap[b]/eV	H_2 evolution rate[c]/mmol $\hbar^{-1}$ g^{-1}
0	2.64	1.85
0.5%	2.57	2.81
1.0%	2.48	2.94
1.5%	2.47	3.20
2.0%	2.45	2.58
3%	2.41	1.94

[a] Calculated from the atomic ratio of the $Ag^+/(In^{3+}+Zn^{2+})$ in the starting materials. [b] The band gaps are calculated by $(Ahv)^{1/2} \sim hv$ plot based on the absorbance of the UV-vis DRS. [c] Catalysts, 0.1 g; reactant solution, 100 mL aqueous solution containing 0.35 M Na_2S and 0.25 M Na_2SO_3 as sacrificial reagents with 0.5 wt% Ru loaded as co-catalyst; light source, 300 W Xenon lamp with a cut-off filter ($\lambda \geq 420$ nm); the H_2 evolution rates are calculated by the average rate in the first five hours.

classic work[40]. Obviously, the detailed compositions will strongly influence the photocatalytic activity.

As we know, metal ion doping is a very important strategy in photocatalysis, especially in photocatalytic water splitting. Currently, two possible mechanisms are suggested to explain the photocatalytic process. The first one is that metal ion dopants creat donor levels in the forbidden band of the photocatalysts, which can expand the range of light absorption.[31, 32] That is to say, additional photogenerated electron transition happen from the donor levels to the conduction band of the photocatalysts. In our work, Ag4d donor levels are supposed to be created above the valence band of $ZnIn_xS_{1+1.5x}$ solid solution, from which the electrons can be photoexcited to the conduction band, as shown in Fig 8a. Therefore, the photocatalytic activities are enhanced by this way. The second mechanism is that the donor levels contributed by doping ions can trap the photogenerated holes and facilitate the charge separation and transfer.[38, 41] Therefore, all the doped samples exhibit higher H_2 evolution rates than those of the un-doped samples.

In order to find which mechanism may play a key role in our photocatalyst systems, the dependence of H_2 evolution rates of Ag(1.5%)-$ZnIn_{1.5}S_{3.2575}$ on the wavelengths of the different cut-off filters were carried out, as shown in Fig. 8b. The H_2 evolution

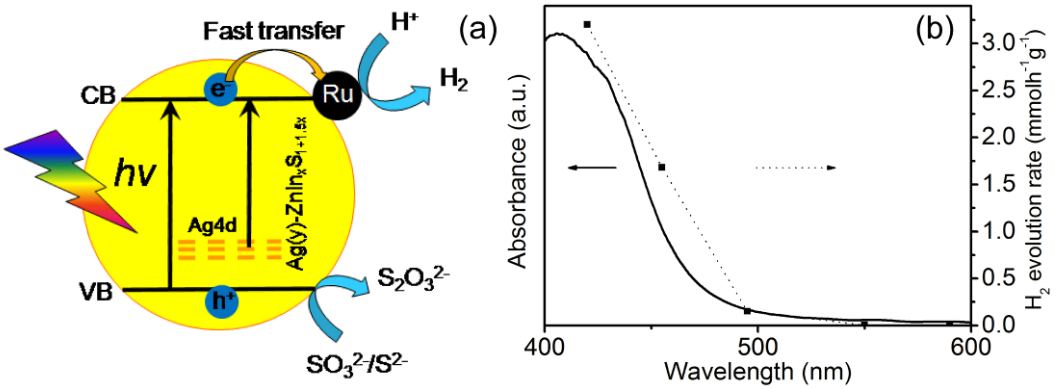

Fig. 8 (a) The mechanism of water reduction to H_2 evolution and sacrificial reagent oxidation on the surface of Ag(y)-$ZnIn_xS_{1+1.5x+0.5y}$ solid solution; (b) Dependence of the H_2 evolution rates on the wavelengths of the cut-off filter for Ag(1.5%)-$ZnIn_{1.5}S_{3.2575}$ sample. Reaction conditions: 0.1 g of Ag(1.5%)-$ZnIn_{1.5}S_{3.2575}$ sample prepared by adding 1 mL hydrochloric acid at 160 ℃ for 6 h in 100 mL aqueous solution containing 0.35 M Na_2S and 0.25 M Na_2SO_3 as sacrificial reagents with 0.5 wt% Ru loaded as co-catalyst, 300 W Xenon lamp with different cut-off filter ($\lambda \geq 420$ nm, 455 nm, 495 nm, 550 nm, 590 nm). The H_2 evolution rates are calculated by the average rate of the first three hours, with 0.5 wt% Ru loaded as co-catalyst.

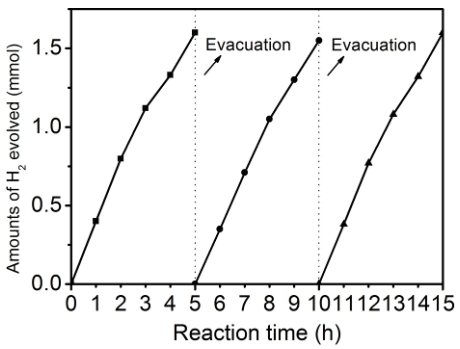

Fig. 9 Stability test of Ag(1.5%)-$ZnIn_{1.5}S_{3.2575}$ sample prepared by adding 1 mL hydrochloric acid at 160 ℃ for 6 h.

rates obtained with 420 and 455 nm cut-off filters are 3.20 and 1.68 mmol h^{-1} g^{-1}, respectively, whereas the H_2 evolution rates for 495 nm, 550 and 590 nm cut-off filters are only 0.15, 0.005 and 0 mol h^{-1} g^{-1}, respectively. These results reveal that the enhancement of H_2 evolution rates by Ag^+ doping mainly takes place in the short-wavelength range (≤ 495 nm), close to the intrinsic absorption region of $ZnIn_{1.5}S_{3.25}$ solid solution. Therefore, it is believed that the enhancement is primarily ascribed to the promotion of the photogenerated charge separation and transfer in the intrinsic absorption region of Zn-In-S solid solution. Besides, the onset of the action spectrum of H_2 evolution rate is consistent with the diffuse reflectance spectrum, indicating that Ag4d donor levels participate the formation of the energy structure of the doped solid solution and the visible light absorption of the photocatalyst comes from the transition between Ag4d donor levels and the conduction band of the solid solution.[42, 43] Besides, the Ag(1.5%)-$ZnIn_{1.5}S_{3.2575}$ solid solution exhibits good stability, as shown in Fig. 9. The doped sample can show quite stable H_2 evolution activity without abvious decrease in the first three circles. The slight drop in the H_2 evolution rate may be due to the consumption of the sacrificial reagents in three circles reaction.[30]

Conclusions

In summary, two series of $ZnIn_xS_{1+1.5x}$ solid solution and Ag(y)-$ZnIn_xS_{1+1.5x+0.5y}$ solid solution are prepared by hydrotheraml method. The photocatalytic H_2 evolution rates were greatly influenced by synthetic conditions of the photocatalysts, such as the In/Zn molar ratios, the amount of hydrochlorid acid added before the hydrothermal reaction, hydrothermal temperature and reaction time. 1.85 mmol h^{-1} g^{-1} of H_2 evolution rate was obtained for the $ZnIn_{1.5}S_{3.25}$ solid solution, which is based on the In/Zn the molar ratio of 1.5 at 160 for 6 h by adding 1 mL hydrochloric acid before the hydrothermal reaction. Further Ag^+ doping can bring higher H_2 evoluion rate of 3.20 mmol h^{-1} g^{-1} for Ag(1.5%)-$ZnIn_{1.5}S_{3.2575}$ sample. This work provides a new opportunity to develop novel efficient photocatalysts by transition metal ions doping.

Acknowledgements

The work was financially supported by the National Natural Science Foundation of China (21173260, 51072221 and 91233202), the Knowledge Innovation Program of the Chinese Academy of Sciences and the National Basic Research Program of China (973 project, 2012CB932903 and 2012CB932904).

Notes and references

[a] *Key Laboratory for Renewable Energy, Chinese Academy of Sciences; Beijing Key Laboratory for New Energy Materials and Devices; Beijing National Laboratory for Condense Matter Physics, Institute of Physics, Chinese Academy of Sciences, Beijing, China. Fax: +86-10-82649242; Tel: +86-10-82649242; E-mail: qbmeng@iphy.ac.cn, dmli@iphy.ac.cn*
[b] *Key Laboratory of Bio-Inspired Smart Interfacial Science and Technology of Ministry of Education, Beijing Key Laboratory of Bio-inspired Energy Materials and Devices, School of Chemistry and Environment, Beihang University, Beijing 100191, PR China.*
† Electronic Supplementary Information (ESI) available: [More information of XRD patterns, SEM images, X-ray energy dispersive spectroscopy (XEDS) maps and XPS characterization]. See DOI: 10.1039/b000000x/

1. A. Fujishima and K. Honda, *Nature*, 1972, **238**, 37.
2. N. S. Lewis, *Nature*, 2001, **414**, 589.
3. Z. Zou, J. Ye, K. Sayama and H. Arakawa, *Nature*, 2001, **414**, 625.
4. K. Maeda, K. Teramura, D. Lu, T. Takata, N. Saito, Y. Inoue and K. Domen, *Nature*, 2006, **440**, 295.
5. H. Kato, K. Asakura and A. Kudo, *J. Am. Chem. Soc.*, 2003, **125**, 3082.
6. M. Matsumura, Y. Saho and H. Tsubomura, *J. Phys. Chem.*, 1983, **87**, 3807.
7. N. Bao, L. Shen, T. Takata and K. Domen, *Chem. Mater.*, 2007, **20**, 110.
8. H. Yan, J. Yang, G. Ma, G. Wu, X. Zong, Z. Lei, J. Shi and C. Li, *J. Catal.*, 2009, **266**, 165.
9. R. Williams, *J. Chem. Phys.*, 1960, **32**, 1505.
10. G. Chen, D. Li, F. Li, Y. Fan, H. Zhao, Y. Luo, R. Yu and Q. Meng, *Appl. Catal. A Gen.*, 2012, **443–444**, 138.
11. G. Chen, F. Li, Y. Fan, Y. Luo, D. Li and Q. Meng, *Catal. Commun.*, 2013, **40**, 51.
12. Y. Wang, Y. Wang and R. Xu, *J Phys. Chem. C*, 2012, **117**, 783.
13. Y. Fan, G. Chen, D. Li, F. Li, Y. Luo and Q. Meng, *Mater. Res. Bull.*, 2011, **46**, 2338.
14. J. Hou, C. Yang, H. Cheng, Z. Wang, S. Jiao and H. Zhu, *Phys. Chem. Chem. Phys.*, 2013, **15**, 15660.
15. J. Hou, C. Yang, Z. Wang, S. Jiao and H. Zhu, *RSC Advances*, 2012, **2**, 10330.
16. T.-H. Yu, W.-Y. Cheng, K.-J. Chao and S.-Y. Lu, *Nanoscale*, 2013, **5**, 7356.
17. S.-W. Cao, Y.-P. Yuan, J. Fang, M. M. Shahjamali, F. Y. C. Boey, J. Barber, S. C. Joachim Loo and C. Xue, *Int. J. Hydrogen Energy*, 2013, **38**, 1258.
18. Z. Lei, W. You, M. Liu, G. Zhou, T. Takata, M. Hara, K. Domen and C. Li, *Chem. Commun.*, 2003, **0**, 2142.
19. N. S. Chaudhari, A. P. Bhirud, R. S. Sonawane, L. K. Nikam, S. S. Warule, V. H. Rane and B. B. Kale, *Green Chem.*, 2011, **13**, 2500.
20. J. Zhou, G. Tian, Y. Chen, X. Meng, Y. Shi, X. Cao, K. Pan and H. Fu, *Chem. Commun.*, 2013, **49**, 2237.
21. Y. Li, J. Wang, S. Peng, G. Lu and S. Li, *Int. J. Hydrogen Energy*, 2010, **35**, 7116.
22. B. Chai, T. Peng, P. Zeng and X. Zhang, *Dalton Trans.*, 2012, **41**, 1179.

23. S. Shen, X. Chen, F. Ren, C. Kronawitter, S. Mao and L. Guo, *Nanoscale Res. Lett.*, 2011, **6**, 290.
24. X. Bai and J. Li, *Mater. Res. Bull.*, 2011, **46**, 1028.
25. Y. Chen, S. Hu, W. Liu, X. Chen, L. Wu, X. Wang, P. Liu and Z. Li, *Dalton Trans.*, 2011, **40**, 2607.
26. J. Shen, J. Zai, Y. Yuan and X. Qian, *Int. J. Hydrogen Energy*, 2012, **37**, 16986.
27. D. Jing, M. Liu and L. Guo, *Catal. Lett.*, 2010, **140**, 167.
28. S. Shen, L. Zhao, Z. Zhou and L. Guo, *J Phys. Chem. C*, 2008, **112**, 16148.
29. J. F. Reber and M. Rusek, *J. Phys. Chem.*, 1986, **90**, 824.
30. B. Chai, T. Peng, P. Zeng, X. Zhang and X. Liu, *J Phys. Chem. C*, 2011, **115**, 6149.
31. I. Tsuji, H. Kato, H. Kobayashi and A. Kudo, *J. Am. Chem. Soc.*, 2004, **126**, 13406.
32. I. Tsuji, H. Kato and A. Kudo, *Chem. Mater.*, 2006, **18**, 1969.
33. R. Shannon, *Acta Crystallogr. A*, 1976, **32**, 751.
34. F. Li, G. Chen, J. Luo, Q. Huang, Y. Luo, Q. Meng and D. Li, *Catal. Sci. Technol.*, 2013, **3**, 1993.
35. Y. Li, G. Chen, C. Zhou and J. Sun, *Chem. Commun.*, 2009, 2020.
36. Y. Wang, J. Wu, J. Zheng, R. Jiang and R. Xu, *Catal. Sci. Technol.*, 2012, **2**, 581.
37. K. Ikeue, S. Shiiba and M. Machida, *ChemSusChem*, 2011, **4**, 269.
38. K. Ikeue, Y. Shinmura and M. Machida, *Appl. Catal. B Environ.*, 2012, **123–124**, 84.
39. B. V. R. Chowdari, K. F. Mok, J. M. Xie and R. Gopalakrishnan, *J. Non-cryst. Solids.*, 1993, **160**, 73.
40. I. Tsuji, H. Kato, H. Kobayashi and A. Kudo, *J. Am. Chem. Soc.*, 2004, 126, 13406-13413.
41. M. A. Fox and M. T. Dulay, *Chem. Rev.*, 1993, **93**, 341.
42. H. Zhang, G. Chen, X. He and Y. Li, *Int. J. Hydrogen Energy*, 2012, **37**, 5532.
43. I. Tsuji, Y. Shimodaira, H. Kato, H. Kobayashi and A. Kudo, *Chem. Mater.*, 2010, **22**, 1402.

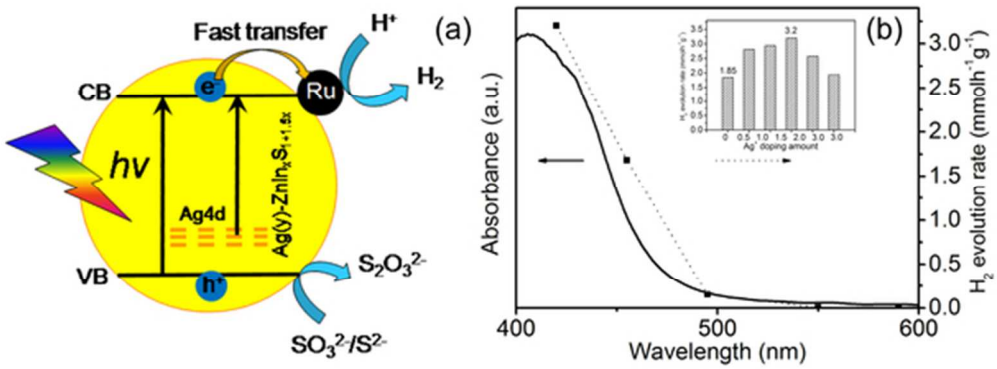

(a) The mechanism of water reduction to H_2 evolution and sacrificial reagent oxidation on the surface of Ag(y)-$ZnIn_xS_{1+1.5x}$ solid solution; (b) Dependence of the H_2 evolution rates on the wavelengths of the cut-off filter for Ag(1.5%)-$ZnIn_{1.5}S_{3.25}$ sample, the inset is the H_2 evolution rate of Ag(y)-$ZnIn_{1.5}S_{3.25}$ samples.
51x18mm (300 x 300 DPI)